Int. J. Advance Soft Compu. Appl, Vol. 10, No. 3, November 2018
ISSN 2074-8523

Effect of Regularization parameter on Total Variation based Denoising of Magnetic Resonance Images

Nikita Joshi[1], Sarika Jain[2], Amit Agarwal[3]

1 Research Scholar, Amity School of Engineering & Technology, Amity University Uttar Pradesh, Noida, India
nikitajoshi502@gmail.com
2 Assistant Professor, Amity Institute of Information Technology, Amity University Uttar Pradesh, Noida, India
ashusarika@gmail.com
3 University of Petroleum and Energy Studies, Dehradun, India

Abstract

Noise affects Magnetic Resonance (MR) images, due to which the problem of inaccurate medical diagnosis occurs. Therefore noise removal is an important task while dealing MR images. In this paper, the discrete total variation method has been discussed and analysed for removing noise from Magnetic Resonance Images. The effect of regularization parameter lambda has been studied for denoising. This method has been extensively experimented with MR images by varying the parameter lambda. The evaluation metrics are Peak Signal to Noise Ratio (PSNR) and Mean Square Error (MSE). The experiment demonstrated that the value of PSNR decreases and MSE increases as the value of lambda increases from 0.01 to 1.0. The noise is reduced and contrast is improved.

Keywords: *Discrete total variation, image denoising, magnetic resonance images, regularization parameter*

1. Introduction

The total variation (TV) regularization method was originally introduced by Rudin, Osher and Fatemi [1]. It is effective in removing noise, recovering sharp images by preserving sharp discontinuities [2, 3, 4]. It can be used in graphs, segmentation and clustering problems as well [5, 6]. Convex optimization methods with primal dual splitting techniques have proved to be useful in implementing TV minimization in an effective manner [3, 7, 8-19]. TV is the l_1 norm of the gradient amplitude for 2-D functions. Condat [20] proposed a new technique as the gradient cannot be defined properly in discrete images. This method, known as discrete TV, preserves edges efficiently. The image is associated with a gradient field on a twice finer grid. The l_1 norm of the gradient amplitude is found out for calculating the TV. TV method is now used in many applications like regularizing parallel imaging [21, 22], reduction of truncation artefacts in MR images [23], process of inpainting on sensitivity maps [24], regularizing undersampled imaging methods [25] and reconstructing and sampling of radial MRI data [26, 27].

In this paper, the effect of regularization parameter on discrete TV method discussed by Condat [20], has been studied and used particularly for removing noise from MR images. In Sec. 2 we discuss the existing definitions of discrete TV along with the new definition proposed by Condat [20] with its primal and dual formulation. In Sec. 3, the TV minimization algorithm used for MR images is discussed. Sec. 4 deals with the noise in MR images. In Sec. 5, the experiment has been performed and its effects have been studied on varying the regularization parameter. The conclusion has been stated in Sec.6.

2. Theory

2.1 Various definitions of discrete TV

A function $u(t_1,t_2)$ defined in the plane $\mathbb{R}^2$ possesses a gradient field $\nabla u(t_1, t_2)=\left(\frac{\partial u}{\partial t_1}(t_1,t_2), \frac{\partial u}{\partial t_2}(t_1,t_2)\right)$ also in the plane $\mathbb{R}^2$. Thus TV is defined as the $l_{1,2}$ norm of the gradient and is given as

$$TV(u)= \int_{R^2} |\nabla u(t_1,t_2) dt_1\, dt_2| \quad (1)$$

The TV is isotropic in nature.
In the entire paper, i is a grayscale discrete image of size $N_1 X\, N_2$ and having pixel values $i(n_1, n_2)$, defined at pixel location n_1, n_2 and lying in the domain $\Omega=\{1,\ldots\ldots N_1\}X\{1,\ldots\ldots N_2\}$, where n_1 and n_2 represent the row and column

indices. The anisotropic TV is a kind of discrete TV and is defined as follows, assuming the boundary conditions to be Neumann, i.e. symmetric in nature and any finite difference over the boundary is zero.

$$TV_a(i)=\sum_{n_1}^{N_1}\sum_{n_2}^{N_2}|i[n_1+1,n_2]-i[n_1,n_2]|+|i[n_1,\ n_2+1]-i[n_1,n_2]| \quad (2)$$

This definition of anisotropic TV is inefficient as it results in metrication artefacts. To avoid this, one uses isotropic TV, defined as follows

$$TV_i(i)=\sum_{n_1}^{N_1}\sum_{n_2}^{N_2}\sqrt{(i[n_1+1,n_2]-i[n_1,n_2])^2+(i[n_1,n_2+1]-i[n_1,n_2])^2} \quad (3)$$

This definition of isotropic TV also uses Neumann boundary conditions.

The TV of the image should remain unaltered on a rotation of ±90º, or on flipping horizontally or vertically. Condat in [20] shows that this does not happen with isotropic TV and a change factor of $\sqrt{2}$ occurs with a horizontal flip. But still it has been seen that the isotropic TV is largely used because of its simplicity. To maintain the four-fold symmetry, the image is rotated by 0 º, ±90º and 180 º and then TV_i is applied on the rotated images, and henceforth the average is taken of all the four TV_i results respectively. But still in this case too, the oblique edges get blurred and any checkerboard pattern or an isolated pixel gives very low value.

A more isotropic TV has been discussed in [28] , called the upwind TV and is defined as follows

$$TV_u(i)=\sum_{n_1}^{N_1}\sum_{n_2}^{N_2}\sqrt{\begin{matrix}(i[n_1,n_2]-i[n_1+1,n_2])^2{}_+ + (i[n_1,n_2]-i[n_1-1,n_2])^2{}_+ + \\ (i[n_1,n_2]-i[n_1,n_2+1])^2{}_+ + (i[n_1,n_2]-i[n_1,n_2-1])^2{}_+\end{matrix}} \quad (4)$$

Where x_+ denotes $\max(i,0)$. Although this upwind TV demonstrates more isotropic nature and does not blur the oblique edges, it varies on taking the negative of the image.

Abergel [29] proposed the Shanon total variation. In this method, the Shanon interpolate of the image is found and then its continuous total variation is estimated. This is performed by using Riemann sum approximation. This method removes aliasing but at the same time blurriness is introduced in the image.

2.2. Dual and Primal formulation of discrete TV by Condat

2.2.1 Dual Formulation

The dual formulation of TV of a function a can be defined in continuous domain as

$$TV(a)=\sup\{\langle a,-\mathrm{div}(b)\rangle : b \in C_c^1(R^2,R^2),\ |b(x)|\leq 1\ \forall\ t\in R^2\} \quad (5)$$

Where div denotes the divergence operator, $C_c^1(R^2,R^2)$ denotes the set of continuously differentiable function ranging from $\mathbb{R}^2$ to $\mathbb{R}^2$ and having a compact support, and. The amplitude of the dual variable x is bounded by 1 all over.

Similarly the dual formulation of TV can be defined in the discrete domain also. In the discrete domain, a discrete operator Z is defined which maps the image $i \in R^{N1\ X\ N2}$ to the vector field $Z\ i \in (R^2)^{N_1\ X\ N_2}$. The discrete operator Z is defined as the forward finite differences of the image i, and is given as

$$(Zi)_1[n_1,n_2]=i[n_1+1, n_2]-i[n_1, n_2] \quad (6)$$

$$(Zi)_2[n_1,n_2]=i[n_1, n_2+1]-i[n_1, n_2] \quad (7)$$

for every $(n_1,n_2)\in\Omega$ and having the Neumann boundary conditions.

For convenience it is considered that all the images under consideration and the vector fields have similar size $N_1\ X\ N_2$ and are indexed by $(n_1,n_2)\in\Omega$, considering that some of the last row or column value is zero and are constant, i.e. $(Zi)_1[N_1,n_2]=(Zi)_2[n_1,N_2]=0$ for every $(n_1,n_2)\in\Omega$. So TV_i can be defined as $TV_i(i)=\|Zi\|_{1,2}$ where the $l_{1,2}$ norm denotes the sum over the indices n_1, n_2 of the 2-norm $|(Zi)[n_1, n_2]|$

Thus the dual formulation of the isotropic TV of image i is defined as

$$TV_i(i)= \max_{x\in(R^2)^{N_1\ X\ N_2}} \{\langle Zi,x\rangle : |x[n_1, n_2]| \leq 1\ \forall\ (n_1, n_2) \in \Omega\} \quad (8)$$

and having Euclidean inner product.

Condat proposed to correct the pixel shift in the isotropic TV by using interpolation. The pixel shift is taken to be of half pixel. The dual images x_1 and x_2 having values $x_1[n_1, n_2]$ and $x_2[n_1, n_2]$ are located at pixel edges $\left(n_1+\frac{1}{2},\ n_2\right)$

and $\left(n_1,\ n_2+\frac{1}{2}\right)$ respectively, so that when the pixels are interpolated, the constraint $|x[n_1, n_2]|\leq 1$ is satisfied at the pixel edges as well as at the pixel centres. Thus the dual formulation of TV as proposed by Condat is

$$TV_c(i)=\max_{x\in(R^2)^{N_1 X N_2}}\left\{\begin{matrix}\langle Zi,x\rangle \\ : \left|(L_{\updownarrow}x)[n_1, n_2]\right|\leq 1,\ |(L_{\leftrightarrow}x)[n_1, n_2]|\leq 1,\ |(L_{\blacksquare}x)[n_1, n_2]|\end{matrix}\right\} \tag{9}$$

Where $L_{\updownarrow}$, $L_{\leftrightarrow}$, and $L_{\blacksquare}$ are the bilinear interpolation operators applied on the image pair $x=(x_1, x_2)$ on the grids $\left(n_1+\frac{1}{2},\ n_2\right)$, $\left(n_1,\ n_2+\frac{1}{2}\right)$, (n_1, n_2), for $(n_1, n_2)\in\Omega$ respectively. The interpolation operators as defined by Condat in [20] are as follows:

$$(L_{\updownarrow}x)_1[n_1, n_2]=x_1[n_1, n_2] \tag{10}$$
$$(L_{\updownarrow}x)_2[n_1, n_2]=(x_2[n_1, n_2]+x_2[n_1, n_2\text{-}1], x_2[n_1+1, n_2]+x_2[n_1+1, n_2\text{-}1])/4 \tag{11}$$
$$(L_{\leftrightarrow}x)_1[n_1, n_2]=(x_1[n_1, n_2]+x_1[n_1\text{-}1, n_2], x_1[n_1, n_2+1]+x_1[n_1\text{-}1, n_2+1])/4 \tag{12}$$
$$(L_{\leftrightarrow}x)_2[n_1, n_2]=x_2[n_1, n_2] \tag{13}$$
$$(L_{\blacksquare}x)_1[n_1, n_2]=(x_1[n_1, n_2]+x_1[n_1\text{-}1, n_2])/2 \tag{14}$$
$$(L_{\blacksquare}x)_2[n_1, n_2]=(x_2[n_1, n_2]+x_2[n_1, n_2\text{-}1])/2 \tag{15}$$

For all $(n_1, n_2)\in\Omega$

Combining the three operators $L_{\updownarrow}$, $L_{\leftrightarrow}$ and $L_{\blacksquare}$ by the linear operator L, and taking the $l_{\infty,\infty,2}$ norm $\|\cdot\|_{\infty,\infty,2}$ of a field as the maximum value among the three components and the pixels of the 2-norm of its vectors. Thus eq. (8) can be rewritten as

$$TV_c(i)=\max_{x\in(R^2)^{N_1 X N_2}}\{\langle Zi, x\rangle : \|Lx\|_{\infty,\infty,2}\leq 1\} \tag{16}$$

2.2.2 Primal Formulation

Condat proposed the primal formulation of the discrete TV equivalent to the dual formulation in eq. (9)

$$TV_c(i)=\min_{y_{\updownarrow}, y_{\leftrightarrow}, y_{\blacksquare}\in(R^2)^{N_1 X N_2}}\left\{\left\|y_{\updownarrow}\right\|_{1,2}+\left\|y_{\leftrightarrow}\right\|_{1,2}+\left\|y_{\blacksquare}\right\|_{1,2} : L^*_{\updownarrow}y_{\updownarrow}+L^*_{\leftrightarrow}y_{\leftrightarrow}+L^*_{\blacksquare}y_{\blacksquare}=Zi\right\} \tag{17}$$

Where $.^*$ represents the adjoint operator. $y_{\updownarrow}$, $y_{\leftrightarrow}$, $y_{\blacksquare}$ denote the vector field.

The above equation (17) can be redefined more compactly by combining the three vector fields $y_{\updownarrow}, y_{\leftrightarrow}, y_{\blacksquare}$ and replacing by vector field y. The sum of the $l_{1,2}$ norm of the three components $y_{\updownarrow}, y_{\leftrightarrow}, y_{\blacksquare}$ can be denoted by $l_{1,1,2}$ norm of y. There exists $L^{*}y=L^{*}_{\updownarrow}y_{\updownarrow}+L^{*}_{\leftrightarrow}y_{\leftrightarrow}+L^{*}_{\blacksquare}y_{\blacksquare}$ Then Eq. (17) can be rewritten as

$$TV_c(i)=\min_{y\in\left((R^2)^{N_1 X N_2}\right)^3}\{\|y\|_{1,1,2} : L^{*}y=Zi\} \tag{18}$$

Given an image i, y is the vector field which is the combination of $y_{\updownarrow}, y_{\leftrightarrow}, y_{\blacksquare}$. For the image i, having indices $(n_1, n_2)\in\Omega$, its elements $y_{\updownarrow}[n_1, n_2], y_{\leftrightarrow}[n_1, n_2], y_{\blacksquare}[n_1, n_2]$ are vectors of $\mathbb{R}^2$, located at the positions $\left(n_1+\frac{1}{2}, n_2\right)$, $\left(n_1, n_2+\frac{1}{2}\right), (n_1, n_2)$.Then y is the gradient field of i. Thus, the definition of discrete TV proposed by Condat in eq.(16), is the $l_{1,2}$ norm of the gradient field y of the image i.

3. Discrete TV used for denoising MRI

The discrete TV proposed by Condat in [20] in the above section can be applied on MR images and used for denoising MRI.
The regularization parameter λ is varied keeping the value of μ=1. The algorithm used for MR images is discussed below.

3.1 TV Minimization Algorithm

The general convex optimization problem says

$$\text{Find } \hat{i}\in\arg\min_{i\in R^{N_1 XN_2}}\{F(i)+\lambda\, TV(i)\} \tag{19}$$

Where the image *i* is of size N_1 X N_2 and λ is the regularization parameter such that λ>0. F is a convex function which is semi continuous.
When image j is given, we can solve

$$\text{Find } \hat{i}\in\arg\min_{i\in R^{N_1 XN_2}}\left\{\frac{1}{2}\|i-j\|^2+\lambda\, TV(i)\right\} \tag{20}$$

where the norm function denotes the Euclidean norm.
Given an image j and a linear operator A, many inverse problems can be written as

$$\text{Find } \hat{i}\in\arg\min_{i\in R^{N_1 XN_2}}\left\{\frac{1}{2}\|Ai-j\|^2+\lambda\, TV(i)\right\} \tag{21}$$

Many primal-dual algorithms exists which efficiently solve the problems of the form of eq.(18); see, e.g.[3, 17, 18]. Condat has used the over relaxed version [30] of the algorithm in [3]. The convex optimization problem in eq.(19)can be drafted as

$$\text{Find } (\hat{i},\hat{y}) \in \underset{i\in R^{N_1 XN_2}, y\in((R^2)^{N1XN2})^3}{\arg\min} \{F(i)+\lambda \|y\|_{1,1,2} : \quad L^* y=Di\} \tag{22}$$

The image $\hat{i}$ as well as its gradient field $\hat{y}$ has to be found.
Eq.(22) can be generalised as

$$\text{Find } (\hat{i},\hat{y}) \in \underset{i\in R^{N_1 XN_2}, y\in((R^2)^{N1XN2})^3}{\arg\min} \{F(i)+G(y) : Cy+Di=0\} \tag{23}$$

where the function $G(y)= \lambda \|y\|_{1,1,2}$ and $C=-L^*$, C being a linear operator.

As discussed in [31, 32, 33], proximity operator can be applied for any parameter $\alpha>0$. For performing denoising using eq. (20), the proximity operator is: $\text{prox}_{\alpha F}(i)=(i+\alpha y)/(1+\alpha)$. Algorithm 1 can be used to solve eq.(22)

Algorithm 1

1. Select the parameters τ, γ and μ such that $0<\tau<1/\|Z\|^2$, $0<\gamma<1/\|C\|^2$, $\mu>0$ and the initial estimates $i^{(0)}$, $y^{(0)}$,$x^{(0)}$
2. Repeat for p=0, 1…..

$$i^{(p+1)}=\text{prox}_{\tau\mu F}\left(i^{(p)}-\tau Z^*\left(Zi^{(p)}+ Cy^{(p)}+\mu x^{(p)}\right)\right)$$

$$y^{(p+1)}=\text{prox}_{\gamma\mu G}(y^{(p)}-\gamma C^*\left(Zi^{(p+1)}+ Cy^{(p)}+\mu x^{(p)}\right))$$

$$x^{(p+1)}=x^p+\left(Zi^{(p+1)}+Cy^{(p+1)}\right) / \mu$$

It is assumed that the solution to eq.(22) exists when the minimizer of function F exists and algorithm 1 converges [33, 34]; the variables $i^{(p)}$, $y^{(p)}$,$x^{(p)}$ converge to some $\hat{i}$, $\hat{y}$, $\hat{x}$.

The gradient field y of the image i (solving eq.(17)), can be computed by Algorithm 2

Algorithm 2

1. Select the parameters $\boldsymbol{\tau}$ and $\boldsymbol{\mu}$ such that $0<\tau<1/\|C\|^2$ and $\mu>0$; and the initial estimates $y^{(0)}$,$x^{(0)}$
2. Repeat for p=0, 1…..

$$y^{(p+1)}=\text{prox}_{\gamma\mu G}\left(y^{(p)}-\gamma C^{*}\left(Zi+Cy^{(p)}+\mu x^{(p)}\right)\right)$$
$$x^{(p+1)}=x^{(p)}+\left(Zi+Cy^{(p+1)}\right)/\mu$$

To solve eq.(21) which is a regularized least-square problem, Algorithm 1 needs to be modified because it is difficult to find the proximity operator of the quadratic term. A fully split algorithm has to be obtained. So considering a general problem

$$\text{Find } \hat{i}\in \underset{i\in R^{N_1XN_2}}{\arg\min}\left\{F(i)+\frac{1}{2}\|Ai-j\|^2+\lambda\, TV_c(i)\right\} \tag{24}$$

or equivalently the above eq.(24) can be expressed as

$$\text{Find } (\hat{i},\hat{y})\in \underset{i\in R^{N_1XN_2},y\in\left((R^2)^{N_1XN_2}\right)^3}{\arg\min}\left\{F(i)+\frac{1}{2}\|Ai-j\|^2+G(y)\;\; Cy+Di=0\right\} \tag{25}$$

Where $G(y)=\lambda\|y\|_{1,1,2}$ and $C=-L^{*}$

Algorithm 3 is used to find the solution of (24) and its dual.

Algorithm 3

1. Select the parameters $\tau>0$,$\mu>0$, such that
$\tau<1/(\|Z\|^2+\mu\|A\|^2)$, $0<\gamma<1/\|C\|^2$ and the initial estimates $i^{(0)}$, $y^{(0)}$,$x^{(0)}$
2. Repeat, for p=0,1…..

$$i^{(p+1)}=\text{prox}_{\tau\mu F}\left(i^{(p)}-\tau Z^{*}\left(Zi^{(p)}+Cy^{(p)}+\mu x^{(p)}\right)-\tau\mu A^{*}\left(Ai^{(p)}-j\right)\right)$$
$$y^{(p+1)}=\text{prox}_{\gamma\mu G}\left(y^{(p)}-\gamma C^{*}\left(Zi^{(p+1)}+Cy^{(p)}+\mu x^{(p)}\right)\right)$$
$$x^{(p+1)}=x^{(p)}+(Zi^{(p+1)}+Cy^{(p+1)})/\mu$$

4. Noise in MR images

Noise in MR images is a great obstruction in the correct diagnoses. The MR images are often corrupted by the signal dependent white Gaussian noise. The noise in MR images generally gets added at the time of image acquisition. In addition to the patient's thermal noise, noise also gets added through the frequency coils and preamplifiers. Image analysis such as registration and segmentation is greatly affected by noise. Thus the noise introduced should be minimized with the least alteration in the original signal. It is considered that the noise is complex Additive White Gaussian Noise (AWGN), has zero mean and is

independent of the signal [35]. The Gaussian distribution is bell-shaped with a single peak (Fig.1) [36], and is symmetric in nature. Considering a random variable a, with mean m, and variance v^2, it follows a Gaussian distribution P(a) given below in eq.(26) [36].

$$P(a)=\frac{1}{v\sqrt{2\pi}}e^{-(x-m)^2/(2v^2)} \text{ on } a = (-\infty, \infty) \tag{26}$$

For reconstructing the MR image, the raw data is firstly altered by applying 2-D Fourier transform on it, which retains the shape of the raw data. The absolute value $|mg[u_1,v_1]|$ is found for each pixel as given below in eq.(27).

$$|Mg[u_1,v_1]|=\left[\begin{matrix}\left(s[u_1,v_1]\cos(\phi)+\eta_{RE}[u_1,v_1]\right)^2+\\ \left(s[u_1,v_1]\sin(\phi)+\eta_{IM}[u_1v_1]\right)^2\end{matrix}\right]^{\frac{1}{2}} \tag{27}$$

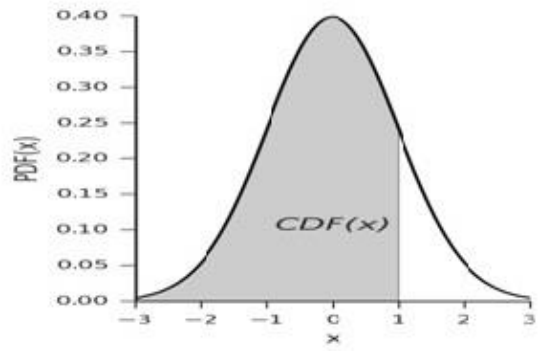

Fig.1 The probability function of the Gaussian distribution [37]

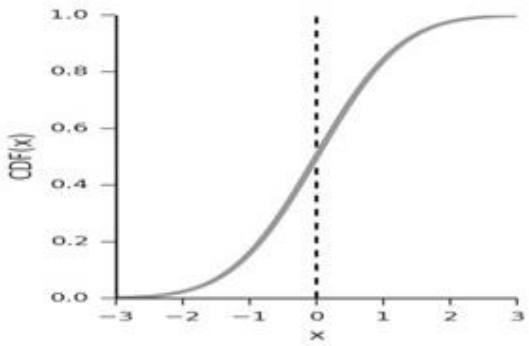

Fig.2 Corresponding cumulative function of Gaussian Distribution [37]

where $|mg[u_1,v_1]|$ denotes the magnitude signal of pixel $[u_1,v_1]$, $s[u_1,v_1]$ is the original signal having phase angle ϕ and η represents the noise that gets added into the real (RE) and imaginary (IM) part of the pixel $[u_1,v_1]$. The original signals as well as noise contribute in the formulation of the magnitude image.

Bayesian approaches [38], wavelet thresholding [40, 41], anisotropic diffusion filter [39], total variation minimization [43] and adaptive smoothing [42] and are some of the popular techniques used for denoising.

4.1 Noise Characteristics in MR images

During the scanning process of MRI, the tissue of the specific area undergo magnetization distribution. Its Fourier transform is the actual data obtained in scanning. It is complex in nature. Inverse Fourier transform is used to reconstruct this data so that it has its magnitude component, phase and frequency component. Taking into account the property of fourier transform such as linearity and orthogonality, the noise that is present in the MR data is assumed to be Gaussian noise, whose real and imaginary parts have equal variance and zero mean [44, 45]. The MRI systems with single coil have a Rician distribution modelling of their magnitude data, thereby changing the PDF of the MR data, and making it signal dependent [45].

The noise estimation in MR image tells about the quality of MR image. The PDF of the MR signal is given as

$$f(M|T)=\frac{M}{\sigma^2}e\left(-\frac{M^2+T^2}{2\sigma^2}\right)I_0\left(\frac{AT}{\sigma^2}\right)u(M) \tag{28}$$

Where T denotes the noise free signal level, I_0 denotes the Bessel function of first kind, magnitude variable of MR image is M, σ^2 is the noise variance and $u(.)$ depicts the Heaviside step function .
With SNR having high values, the Rician distribution tends to a Gaussian distribution, having mean $\sqrt{T^2+\sigma^2}$ and variance σ^2 and is given as

$$f(M|T)\approx\frac{1}{\sigma^2}e\left(-\frac{M^2-\sqrt{T^2+\sigma^2}}{2\sigma^2}\right)u(M) \tag{29}$$

In the MRI scanners which have multiple coil system and have parallel imaging, the noise which is present is inhomogeneous in nature. It may be considered that the complex additive white Gaussian noise, having zero mean, corrupts the original signal. The method of sum of squares (SoS) [46] can be used to obtain the magnitude image if sub-sampling is not carried out.

When the noise components are distributed identically and are independent in nature, non central Chi distribution is followed by the magnitude signal $M_L(x)$ and the PDF [46] is given as:

$$f(M_L|T)=\frac{T_L^{1-L}}{\sigma^2}M_L^L e\left(-\frac{M_L^2+T_L^2}{2\sigma^2}\right)I_{L-1}\left(\frac{A_L T_L}{\sigma^2}\right)u(M_L) \quad (30)$$

Where the number of coils is denoted by L. For value of $L = 1$, the above Eq.(30) reduces to the Rician distribution and having central Chi distribution, given below [46]

$$f(M_L)=\frac{2^{1-L}}{\Gamma(L)}\frac{M_L^{2L-1}}{\sigma^{2L}}e\left(-\frac{M_L^2}{2\sigma^2}\right)u(M_L) \quad (31)$$

5. Experiment and Results

In this section the discrete TV given by Condat is evaluated for varying values of the regularizing parameter lambda.

5.1 Data

MR images of a patient suffering from grade 2 prostate cancer were taken. Fast spin echo T2 weighted axial and coronal images of pelvis were obtained on a dedicated phased array body coil using 3 Tesla high gradient system and correlated with T1 weighted axial images. The images were acquired on an ultra-high Philips Achieva 3.0T TX system which delivers faster scans with high resolutions. The images were viewed on a Philips Dicom Viewer 3. Post contrast T1 W images were acquired in axial, coronal and sagittal plains. The prostatic lesion encountered in the MRI was small and faint in nature.

The first measurement was a T1 weighted echo scan of the pelvis. The contrast agent was injected. Repetition time TR and echo time TE were the sequence parameters. TR=583.1 ms. and TE = 8 ms. for T1 weighted scan and TR=3000 ms. and TE=110 ms. for T2 weighted scan.

5.2 Experiment

The discrete TV method was experimented on the above mentioned T1 and T2 weighted MR images and the behaviour of lambda was noted. The value of lambda was varied from 0.01 to 1. Algorithm 1 was used with 1000 iterations and the value of μ =1. The value of τ was set to 0.123 and that of γ to 0.33. The code was run on MATLAB 2016a. The performance of Algorithm 1 has been evaluated on the PSNR and MSE measures.

5.3 Findings

The PSNR value decreases and MSE increases as the lambda value increases from 0.01 to 16. The image gets blurred when the value of lambda further increases

from 0.16. This can be seen from Table 1 and Table 2, as well as from Fig.3 and Fig. 4. It was observed that for lambda ranging from 0.01 to 1.0, the PSNR values remains the same as for of $\mu = 1$. The value of μ experimented were 0.5, 1, 1.5, 2, 4, 8, 10. Similar is the case with MSE. Moreover the image gets blurred as the value of μ is increased from 1.

Table 1: Effect of Varying Lambda Values for μ=1 for T1 weighted MR Image

S. No.	lambda	PSNR	MSE
1	0.01	88.08	0.0001
2	0.02	84.37	0.0002
3	0.03	83.36	0.0003
4	0.05	82.43	0.0004
5	0.04	81.73	0.0004
6	0.07	80.67	0.0006
7	0.10	79.53	0.0007
8	0.12	78.94	0.0008
9	0.16	77.98	0.001
10	0.20	77.23	0.001
11	0.25	74.82	0.002
12	1.0	73.43	0.003

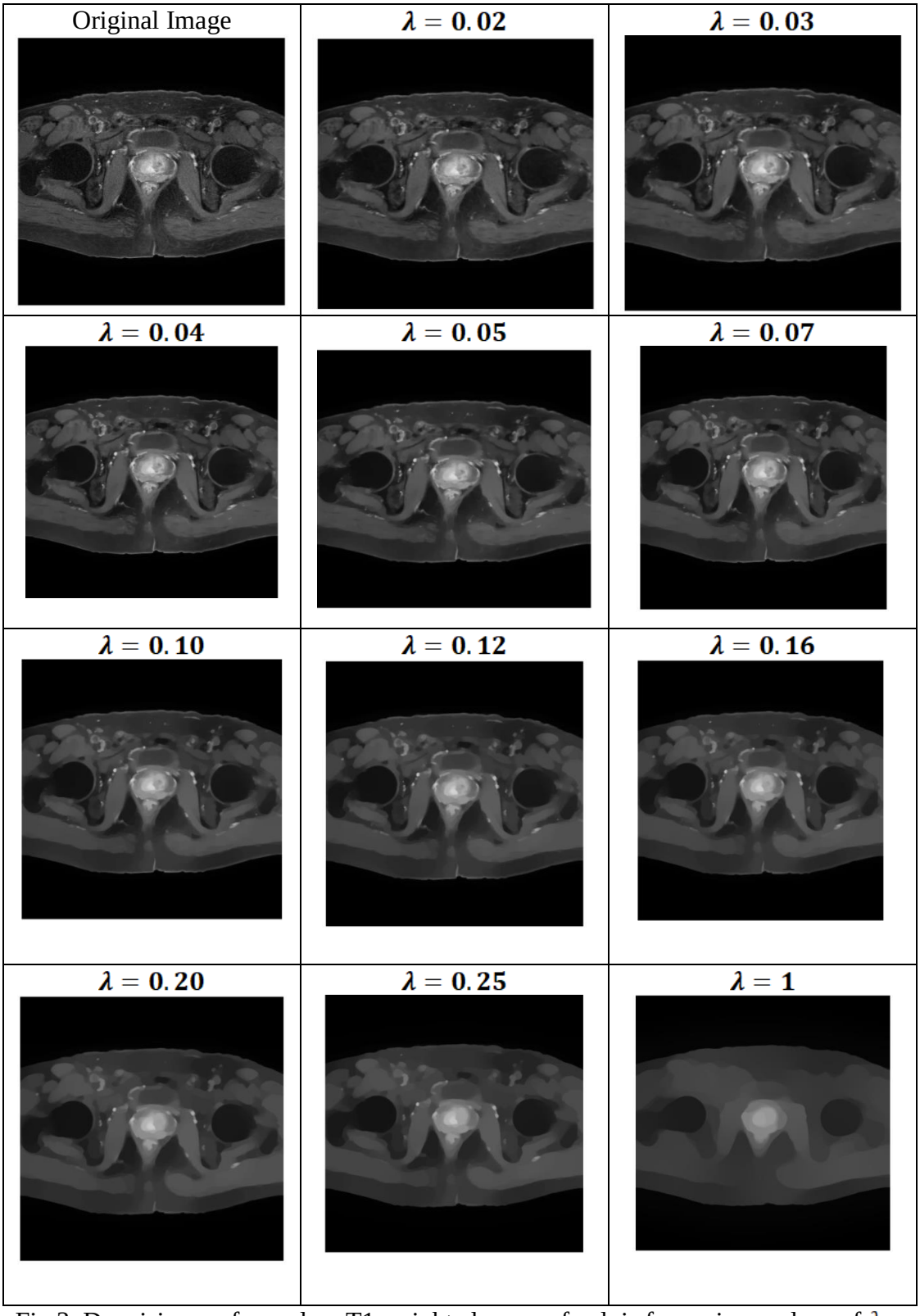

Fig.3. Denoising performed on T1 weighted scans of pelvis for various values of λ

Table 2: Effect of Varying Lambda Values for μ=1 for T2 weighted MR Image

S. No.	lambda	PSNR	MSE
1	0.01	92.23	0.0001
2	0.02	87.89	0.0001
3	0.03	85.63	0.0002
4	0.05	84.10	0.0003
5	0.04	82.97	0.0003
6	0.07	81.36	0.0005
7	0.10	79.77	0.0007
8	0.12	79.09	0.0008
9	0.16	77.90	0.0011
10	0.20	77.10	0.0013
11	0.25	76.35	0.0015
12	1.0	72.16	0.0004

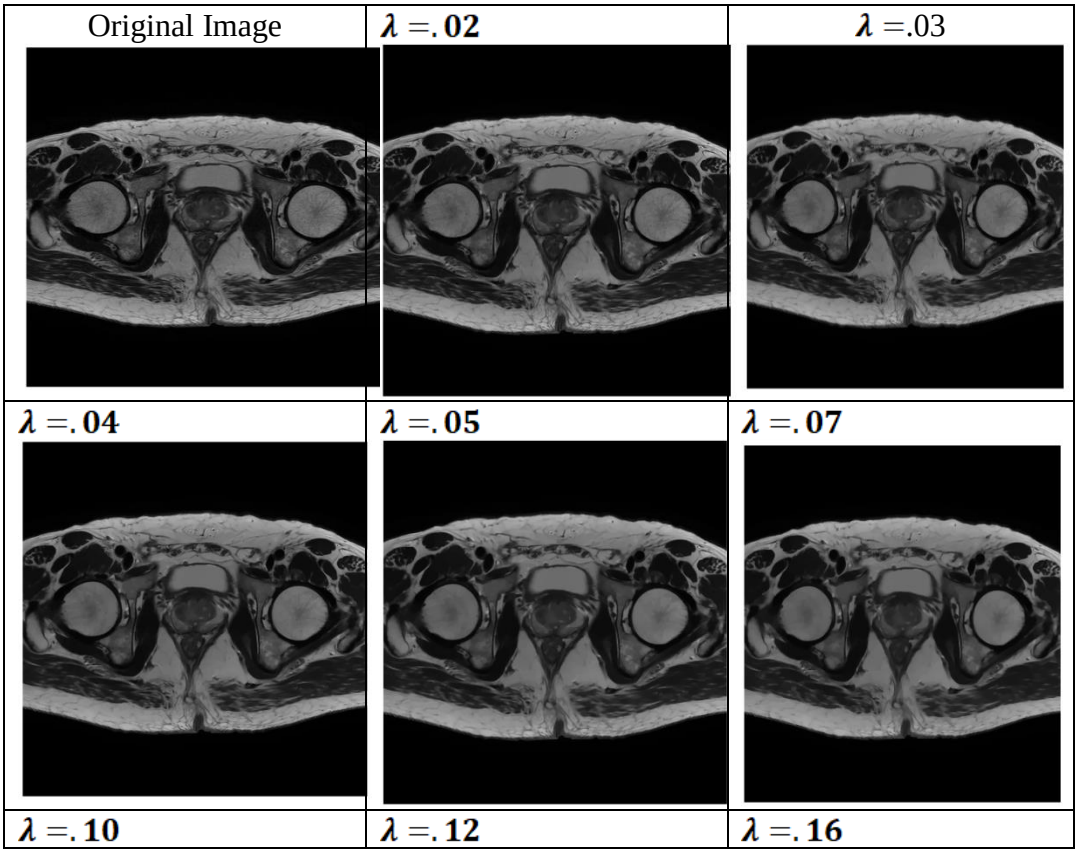

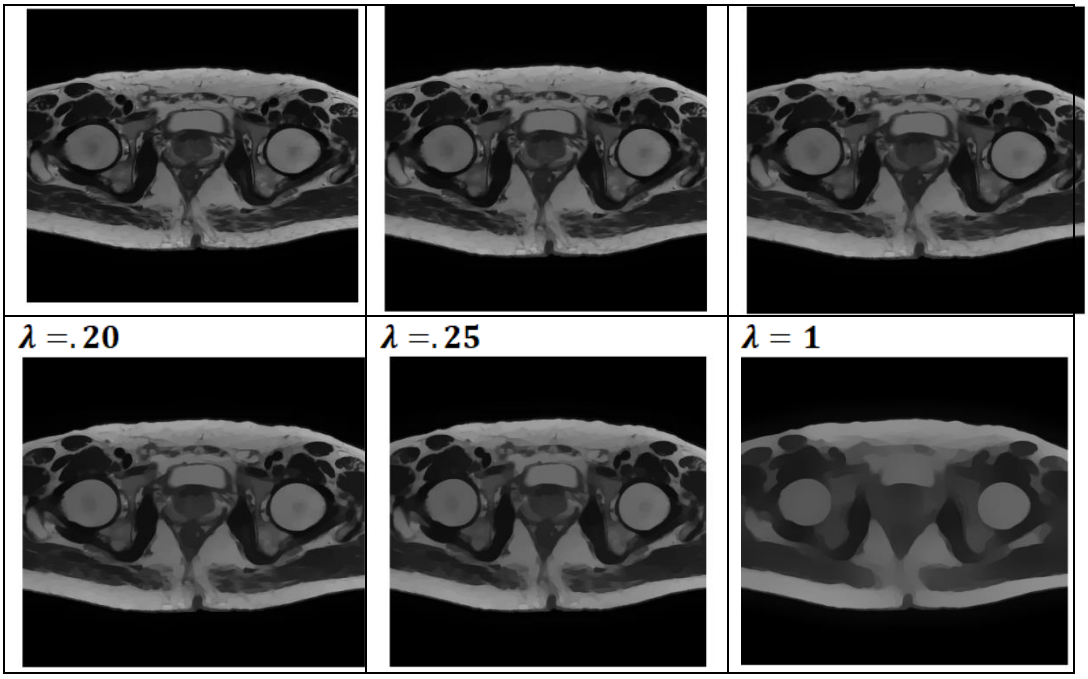

Fig.4. Denoising performed on T2 weighted scans of pelvis for various values of λ.

6. Conclusion

The effect of regularization parameter lambda on the discrete TV method has been discussed in the paper, and has been used for removing noise from T1 and T2 weighted MR images of pelvis. The procedure was evaluated on measures like PSNR and MSE. It has been observed that the value of PSNR increases and MSE decreases as the value of lambda decreases from 1 to 0.01. Noise is significantly removed for lower values of lambda. This method can also be applied to multichannel images or colour images.

ACKNOWLEDGEMENTS

The authors would like to thank Dr. Doda Diagnostics and Healthcare for their support in the axial and coronal MR images.

References

[1] Rudin, L., Osher, S.J.& Fatemi, E. (1992) Nonlinear total variation based noise removal algorithm. *Physica D*, 60, 259–268.

[2] Chambolle, A., Caselles, V., Cremers, D., Novaga, M. & Pock T. (2010). An introduction to total variation for image analysis Theoretical Foundations and Numerical Methods for Sparse Recovery Radon Ser. Comput. *Appl. Math*. 9, 263–340.

[3] Chambolle, A., & Pock T. (2011). A first-order primal-dual algorithm for convex problems with applications to imaging. *J. Math. Imaging Vision*. 40, 120–145.

[4] Burger, M. & Osher, S. (2013). A guide to the TV zoo, in Level Set and PDE Based Reconstruction Methods in Imaging. In *Lecture Notes in Math*. *2090 (*pp. 1–70), Springer, Switzerland.

[5] Goldstein, T., Bresson, I., & Osher S. (2010) Geometric applications of the split Bregman method: Segmentation and surface reconstruction. *J. Sci. Comput*., (45), 272–293.

[6] Chambolle, A., Cremers, D., & Pock, T.(2012). A convei approach to minimal partitions. *SIAM J. Imaging Science*., 5, 1113–1158.

[7] Couprie, C., Grady , L., Najman, L., Pesquet, J.C., & Talbot H. (2013). Dual constrained TV-based regularization on graphs. *SIAM J. Imaging Sci*., 6, 1246-1273.

[8] Goldstein, T. & Osher, S. (2009). The split Bregman method for L1-regularized probs. *SIAM J. Imaging Sci*., 2, 323–343.

[9] Ng, M.K., Weiss, P., & Yuan, I., (2010).Solving constrained total-variation image restoration and reconstruction problems via alternating direction methods", , *SIAM J. Sci. Comput.*, 32, 2710–2736.

[10] Afonso, M., Bioucas J.,Dias, & Figueiredo M. (2010). Fast image recovery using variable splitting and constrained optimization. *IEEE Trans. Image Process*., 19, 2345–2356.

[11] Combettes,L.L., Dung, & Vu, B.C. (2010). Dualization of signal recovery problems. *Set-Valued Var. Anal.* , 18, 373–404.

[12] Zhang, I., Burger, M., & Osher, S. (2011). A unified primal–dual algorithm framework based on Bregman iteration. *J. Sci. Comput.* 46, 20–46.

[13] Briceno-Arias, L.M., & Combettes, P. L. (2011). A monotone skew splitting model for composite monotone inclusions in duality. *SIAM J. Optim*.21, 1230–1250.

[14] Briceno-Arias, L.M., & Combettes, P. L.,Pesquet, J.C., & Pustelnik, L.(2011). Proximal algorithms for multicomponent image recovery problems. *J. Math. Imaging Vision.* 41, 3–22.

[15] Combettes, P. L., Dung, D., & Vu, B. C. (2011). Proximity for sums of composite functions. J. *Math. Anal. Appl.*, 380(2), 680-688.

[16] Vu, B.C. (2013). A splitting algorithm for dual monotone inclusions involving coercive operators. *Adv. Comput. Math*., 38, 667–681.

[17] Condat, L. (2014). A generic proximal algorithm for convex optimization-Application to total variation minimization. *IEEE Signal Processing Lett*., 21, 1054–1057.

[18] Combettes, P.L., Condat, L., Pesquet, J.C. & Vu, B.C. (2014) A forward–backward view of some primal–dual optimization methods in image recovery. In *Proceedings of 21st International Conference on Signal Processing, Paris, France.*(pp. 49-52).

[19] Komodakis, N., Pesquet, J.C. (2015). Playing with duality: An overview of recent primal–dual approaches for solving large-scale optimization problems. *IEEE Signal Processing Mag*., 32, 31–35.
[20] Condat, L. (2017). Discrete Total Variation: New Definition and Minimization. *SIAM Jornal.of Imaging Sciences,* 10(3), 1258-1290.
[21] Liu B, King K, Steckner M, Iie J, Sheng J. &Ying L. (2009). Regularized sensitivity encoding (SENSE) reconstruction using Bregman iterations. *Magn. Reson. Med*, 61,145–152.
[22] Wald M.J., Adluru G., Song H.K., & Wehrli F.W. (2009). Accelerated high-resolution imaging of trabecular bone using total variation constrained reconstruction. In *Proceedings of the 17th Scientific Meeting and Exhibition of ISMRM, Honolulu, HI.*
[23] Block K.T., Uecker M., & Frahm J. (2008). Suppression of MRI truncation artifacts using total variation constrained data extrapolation. In *Proceedings of the 16th Scientific Meeting and Exhibition of ISMRM*, Toronto, Canada.
[24] Huang F., Chen Y., Duensing G.R., Akao J., Rubin A., & Saylor C. (2005). Application of partial differential equation-based inpainting on sensitivity maps. *Magn. Reson. Med*., 53, 388–397.
[25] Lustig M., Donoho D., & Pauly J.M., (2007) Sparse MRI: The application of compressed sensing for rapid MR imaging. *Magn. Reson. Med.*, 58, 1182–1195.
[26] Block K.T., Uecker M., Frahm J., (2007). Undersampled radial MRI with multiple coils. Iterative image reconstruction using a total variation constraint. *Magn. Reson. Med*. 57, 1086–1098.
[27] Block T. (2008).*Advpanced methods for radial data sampling in MRI* (Ph.D. thesis, Georg-August-Universitaet Goettingen).
[28] Chambolle, A., Levine, S.E., B. Lucier, B.J. (2011) An upwind finite-difference method for total variation based image smoothing. *SIAM J. Imaging Sci*., 4, 277-299.
[29] Abergel, R., Moisan, L. (2017) The Shannon total variation. *J.Math. Imaging. Vis.*, DOI.10.1007/s10851-017-0733-5.
[30] Condat, L. (2013). A primal-dual splitting method for convex optimization involving Lipschitzian, proximable and linear composite terms. *J. Optim. Theory Appl.*, 158, 460-479.
[31] Bauschke, H.H., & Combettes, P.L. (2011) Convex Analysis and Monotone Operator Theory in Hilbert Spaces. In *CMS Books in Mathematics*, Springer, New York.
[32] Combettes, P.L., & Pesquet, J.C. (2011). Proximal splitting methods in signal processing, In *Fixed-Point Algorithms for Inverse Problems in Science and Engineering*, (pp.185-212) Springer Publication.
[33] Ma, S. (2016) Alternating proximal gradient method for convex minimization, *J. Sci. Comput*., 68, 546-572.
[34] Deng, W.& Yin, W.(2015). On the global and linear convergence of the generalized alternating direction method of multipliers, *J. Sci. Comput.*, 66, 889-916.

[35] Daessle, N.W., Prima, S., Coupe, P., Morrissey, S.P. & Barillot, C.(2008) Rician noise removal by non-Local Means filtering for low signal-to-noise ratio, MRI: applications to DT-MRI. In *11th Intern. Conf. on Medical Image Computing and Computer-Assisted Intervention*, (pp.171–179).

[36] Bibic, A.(2006) *Denoising of Complex MRI Data by Wiener like Filtering in the Wavelet Domain: Application to High b-value Diffusion Weighted Imaging*. (Master of Science Thesis Medical Radiation Physics Clinical Sciences, Lund University).

[37] Nookala V. (2014). Performance and Evaluation of Guassian Kernals for FCM Algorithm With Mean Filtering Based Denoising For MRI Segmentation. In *Int. Conf. on Communication and Signal Processing*, India,(pp. 1680-1685)

[38] Geman, S., & Geman, D. (1984). Stochastic relaxation Gibbs distribution and the Bayesian restoration of images. *IEEE Trans. Pattern Anal. Mach. Intell*., 6, 721–741.

[39] Perona, P., & Malik, J. (1990) Scale-space and edge detection using anisotropic diffusion. *IEEE Trans. Pattern Anal. Mach. Intell.* 12, 629–639,

[40] Donoho, D.L. (1995). De-noising by soft-thresholding. *IEEE Transact. Informat. Theory*. 41, 613–627.

[41] Donoho D.L., & Johnstone, I.M.(1994). Ideal spatial adaptation by wavelet shrinkage. *Biometrika*. 81(3), 425–455.

[42] Saint Marc, P, Chen, J.S., & Medioni, G. (1991). Adaptive smoothing: a general tool for early vision. *IEEE Trans. Pattern Anal. Mach. Intell.* 13(6), 514–529.

[43] Rudin, L.I., Osher, S., & Fatemi, E. (1992). Nonlinear total variation based noise removal algorithms. *Physica D*. 60, 259–268.

[44] R.M. Henkelman, (1985) Measurement of signal intensities in the presence of noise in MR images, *Med. Phys*. 12, 232–233.

[45] Gudbjartsson, H., & Patz, S.(1995) The Rician distribution of noisy MRI data. *Magn. Reson. Med*. 34, 910–914.

[46] Constantinides, C.D., Atalar, E., McVeigh, E.R.(1997) Signal-to-noise measurements in magnitude images from NMR phased arrays. *Magn. Reson. Med.* 38, 85–857.